# Toward Designing Smart Nanovalves: Modeling of Flow Control through Nanopores via the Helix−Coil Transition of Grafted Polypeptide Chains

**Shashishekar P. Adiga*,† and Donald W. Brenner***

*Department of Materials Science and Engineering, North Carolina State University, Raleigh, North Carolina 27695-7907*

*Received August 2, 2006; Revised Manuscript Received December 13, 2006*

ABSTRACT: Nanopores modified with stimuli-responsive polypeptide chains offer a smart flow-control mechanism. These unique materials have potential wide-ranging applications including smart drug delivery, bioimplants, and molecular machines. Here, we develop a continuum method to analyze flow control through nanopores grafted with polypeptide chains. The helix−coil transition of the polypeptide chains triggered by pH change enables flow regulation. The conformational transition is treated within the Zimm−Bragg model to determine the monomer density profile of the grafted layer inside a nanopore as a function of pH. The Brinkman equation for flow through porous materials is then used to calculate the flow rate. The results are compared with recent experiments in which pH-responsive water permeation through a poly(L-glutamic acid) grafted nanoporous membrane is achieved. The results establish that polymer statistical mechanics combined with a continuum porous layer treatment of flow through the polypeptide grafted nanopore can be used to successfully design smart flow control systems.

## 1. Introduction

Conformational transitions in polypeptides have been a subject of extensive research among molecular biologists. These conformational transitions can be induced by a variety of stimuli including temperature, pH, and ionic concentration. Motivated by the structure−function of biomolecules, a number of nanostructures based on conformational transitions of polypeptide molecules have been envisioned. Park et al., for example, demonstrated a pH responsive nanometer scale gate where a polypeptide brush was grafted into a gold-plated nanoporous membrane.[1] The water permeation through the material was regulated by a helix−coil transformation of the grafted poly(L-glutamic acid) (PLGA) chains in response to pH. At a low pH PLGA has a helical conformation that expands to a random coil conformation as the pH is increased. This transition reduces the effective pore diameter and hence the permeability of the system. Similar signal responsive flow gating has been demonstrated in several other polymer−solvent systems that are triggered by, for example, temperature,[2−4] pH,[5,6] and light.[7] This class of smart materials is of particular interest in smart drug delivery systems,[2] tunable membrane separation,[8] and catalytic reactions.[9] Additionally, one could envision a variety of applications for signal responsive flow control valves in nanotechnology including molecular pumps, solute storage/release system, and chemical to mechanical energy conversion.

In this context, it is important to develop modeling techniques to design polymer grafted nanoporous systems for target applications. It is desirable to determine the conformational transition of the grafted molecules in response to a specific stimulus such as pH, temperature, and the associated change in solvent permeation through the nanoporous system. Recent molecular dynamics (MD)[10] and dissipative particle dynamics (DPD)[11] simulation results have illustrated that grafted polymers offer resistance to flowing particles that changes according to their conformation providing smart flow control functionality to the nanoporous membrane. MD simulations have also been used to investigate modulation of electroosmotic flow through nanopores with grafted polymer chains.[12] While these detailed simulations have provided fundamental information on polymer-flow interaction at the molecular level, they are computationally expensive to apply to design specific polymer−solvent systems. Therefore, it is necessary to develop a continuum hydrodynamic method that incorporates environment-triggerd change in conformation of the grafted molecules to calculate flow control through these smart pores.

In this article, we demonstrate a powerful modeling approach that combines analytic brush structure models, molecular simulation, and continuum fluid mechanics for calculating fluid flow rates through nanopores within which polypeptide chains are grafted. The method is validated by comparing the calculated pH-induced permeability change through PLGA grafted nanopores to the experimental data of Park and co-workers.[1] The monomer density profile of the polypeptide layer as a function of pH is determined using a mean-field polymer brush model that incorporates conformational change due to the helix−coil transition.[13] The necessary molecular parameters for PLGA are deduced from MD simulations of isolated PLGA molecules in water. The change in permeability of a PLGA grafted cylindrical nanopore as a function of pH is then obtained by numerically solving the continuum Brinkman equation for fluid flow.[14] It is demonstrated that such a model is capable of describing the permeability through a PLGA grafted nanopore as a function of pore size, pH, PLGA grafting density, and degree of polymerization.

## 2. Method

**2.1. Outline.** Our model considers flow through a cylindrical nanopore grafted with polypeptide chains. Following earlier continuum calculations,[15] this problem is treated as flow through a porous medium, and the grafted polypeptide chains are

* Corresponding author. E-mail: spadiga@anl.gov, brenner@ncsu.edu.
† Present address: Materials Science Division, Argonne National Laboratory, 9700, S. Cass Ave., Argonne, IL 60439.

10.1021/ma0617522 CCC: $37.00 
Published on Web 01/24/2007

approximated as a polymer brush layer with permeability related to the monomer volume fraction. The resulting Brinkman equation[14] for the system can be written as

$$\frac{1}{r}\frac{\mathrm{d}}{\mathrm{d}r}\left(\mathrm{d}r\frac{\mathrm{d}v_z}{\mathrm{d}r}\right) - \frac{v_z}{k} = \frac{1}{\mu}\frac{\Delta P}{\Delta z} \tag{1}$$

where $r$ is the radial distance from the center of the pore, $\mu$ is the viscosity of the solvent, $\Delta P/\Delta z$ is the pressure drop driving the flow, $v_z$ is the $z$-component of solvent velocity, and $k$ is the permeability of the brush layer. This continuum equation completely describes flow through a cylindrical nanopore grafted with a polymer brush by assigning an infinite $k$ value for the central polymer-free region of the pore (which reduces eq 1 to the Navier−Stokes equation) and a finite value for permeability through the brush layer that is related to the monomer volume fraction $\Phi$ by some function $k(\Phi)$ to be described. It is important to point out that $\Phi$ is not a constant across the grafted layer thickness and in fact has a parabolic profile under good solvent conditions as predicted by self-consistent mean-field theories[16,17] and supported by neutron reflectivity measurements.[18,19] This implies that the permeability $k$ through the grafted layer is a function of $r$. The monomer volume fraction profile $\Phi(r)$ in the brush layer is determined by extending a mean-field analytic brush model[17] to polypeptide chains grafted to a concave surface. This model takes as input the pore size, polypeptide grafting density, number of monomers per chain, monomer repeat length, and Kuhn length.

To incorporate the effect of pH on $\Phi(r)$, conformational change of a polypeptide chain as a function of helical content is calculated in terms of effective monomer repeat length and Kuhn length using the model due to Nagai and Ptitsyn.[20] The helical content as a function of pH in the helix−coil transition region is obtained from the literature.[20,21] Overall, the combination of the statistical mechanical theory of a helix−coil transition and the mean-field theory of polymer brushes provides a technique to determine $\Phi(r)$. Equation 1 is then solved numerically to determine the velocity profile and hence the fluid flow rate through the pore as a function of pH.

**2.2. Conformational Change due to Helix−Coil Transition.** The α-helical configuration is characterized by hydrogen bonding between the carbonyl oxygen of the $i$-th residue and the amide hydrogen of the $(i + 4)$-th succeeding residue.[22,23] This means that the rotation angles, $\varphi$ and $\psi$, for each of the three successive residues must adopt the required values for an α-helix configuration before a hydrogen bond is formed. The helix−random coil transition occurs because the α-helix is favorable energetically due to intramolecular hydrogen bonding, while the random-coil configuration is favorable entropically because of its flexibility.[24] Hence, as the temperature is increased, the entropic contribution to the free energy dominates and a random-coil state is favored. In the case of polypeptide chains with ionizable side chains, a helix−coil transition can be brought about by a change in pH. For example, PLGA, which has a carboxylic acid side chain, is protonated (neutral charge) at a low pH and is deprotonated (negatively charged) at a high pH. In the protonated state, the α-helical structure is favored as compared to a random-coil configuration. In the deprotonated state, the Coulombic repulsion between the negatively charged side chains destabilizes the helical structure and a random coil is favored. In other words, the helix−coil transition of PLGA is controlled by neutral−ionic transition of carboxylic side chains that is driven by a pH change.

The helix−coil transition can be characterized by the fraction of residues $f$ in a polypeptide chain that has helical configuration, i.e., those with $\varphi$ and $\psi$ values corresponding to a helical configuration. In the Zimm−Bragg model, the helix−coil transition is described by two parameters: $s = \exp(-\Delta F/k_BT)$ and $\sigma = \exp(-\Delta F_{init}/k_BT)$.[23,25] The propagation parameter $s$ is associated with adding a helical unit to an already existing helical region. Here $\Delta F$ is the free energy change of a monomer unit accompanying its transition from the free state to the helical state (energy gained due to hydrogen bonding). The initiation parameter $\sigma$ reflects the entropy cost of initiating a helical region. The initiation of a new helical region requires three monomer units to be fixed in a helical configuration as compared to the propagation of an already existing helical region that requires constraining only one monomer segment. This results in extra entropy cost $\Delta F_{init}$. Addition of $m$ monomers to an already existing helical region contributes $m$ hydrogen bonds and costs entropy due to constraining $m$ monomer units, while initiation of a helical region of $m$ monomers contribute $m - 2$ hydrogen bonds and costs entropy of constraining $m$ monomer units. In other words, the presence or absence of a helical conformation in the neighboring monomer units strongly influences the formation of a hydrogen bond in one of the monomer units. For this reason $\sigma$ is also a measure of cooperativity of the helix−coil transition. The degree of cooperativity determines the average number of monomer units in a helical section in the middle of a helix−coil transition region, which is equal to[20]

$$\nu = \exp\left(\frac{F_{init}}{2k_BT}\right) = \frac{1}{\sqrt{\sigma}} \tag{2}$$

From the Zimm−Bragg model, the helical content is given in terms of the above parameters as

$$f = \frac{1}{2}\left(1 + \frac{s-1}{((s-1)^2 + 4\sigma s)^{1/2}}\right) \tag{3}$$

The helix−coil transition in terms of helical content as a function of pH has been investigated both experimentally and theoretically. The experimental methods used for determining the helical content include circular dichroism (CD) and ellipsometry.[20] Zhang et al. have applied an electrostatic model to theoretically determine the effect of pH and salt concentration on the helix content of PLGA chains within the Zimm−Bragg formalism.[21]

**2.3. Monomer Density Profile as a Function of Helical Content.** In this section determination of $\Phi(r)$ of the polypeptide layer as a function of the fraction of helical units ($f$) is described. While $\Phi(r)$ has been calculated for grafted layers of flexible, synthetic polymer chains in the coil−globule transition region using the mean-field approach,[17] to the best of our knowledge, it has not been calculated for a grafted polypeptide brush in the helix−coil transition region. We seek to describe the conformational change of grafted polypeptide chains in the helix−coil transition region using a mean-field approach. In contrast to the coil−globule transition, which is driven by long-range interactions (interaction between monomers farther apart along the chain), the helix−coil transition is cooperative in nature, driven by short-range interactions (hydrogen bonding between neighbors separated by four monomer units). Because of the cooperative nature of the helix−coil transition, the extension of helix−coil transition theory of isolated polypeptide chains to calculate $\Phi(r)$ of densely grafted chains is not straightforward. First, the transition temperature/pH and the width of the transition region are affected by grafting such that the helix state is stabilized,[26,27] and the transition region gets narrower as the

grafting density is increased.[27] Second, the preference for the helical or the coil state of monomers along the grafted chain should depend on the distance from the grafting surface. This is because in a parabolic density profile, a higher density of monomers near the grafting surface causes a greater stretching and hence a preference for helical conformation near the grafted end as compared to the free end. Thus, an exact treatment of the effect of pH on the $\Phi(r)$ incorporating these effects is overwhelming. In our calculations, we ignore (i) the effect of grafting on the helix−coil transition itself and (ii) the distribution of helical segments as a function of distance from the grafting surface. With these simplifications, we calculate the dependence of $\Phi(r)$ on $f$.

The change in overall dimension of an isolated chain as a function of $f$ is quantified in terms of effective monomer repeat length ($a_{\text{eff}}$) and the number of monomers ($p_{\text{eff}}$) in effective Kuhn segment. These effective chain parameters are then used in a mean-field model to calculate $\Phi(r)$. Appendix A details the extension of mean-field calculation for planar brushes to a polypeptide layer grafted on a concave surface. The method can be used to determine $\Phi(r)$ for a set of $R$, grafting density, degree of polymerization, $a_{\text{eff}}$, and $p_{\text{eff}}$ values.

To calculate $a_{\text{eff}}$ and $p_{\text{eff}}$ as a function of $f$, we start with the model due to Nagai and Ptitsyn (refs 20 and 25 and references therein). The model considers a chain in the helix−coil transition region consisting of the helical and random coil sections that are freely linked to one another. A residue in a helical conformation has a length of $l_h = 1.5$ Å in the direction of the helix axis. Thus, a helical segment in the chain can be replaced by a rigid rod of average of $\nu$ residues, i.e., Kuhn length $L_h = \nu l_h$. The random coil section is characterized by a monomer repeat length $l_c = 3.8$ Å and a Kuhn length $L_c = p_c l_c$. Here $p_c$ is the number of monomers in a Kuhn segment of the coil. In a $N$ residue long chain there are $fN$ residues in the helical conformation and $(1 - f)N$ residues in the random coil configuration. The mean-square end-to-end distance ($\langle r^2 \rangle$) of the chain is given by the sum of mean-square end-to-end distances of two hypothetical chains consisting only of coiled sections ($(1 - f)N$ residues) or only of helical sections ($fN$ residues) as follows:

$$\langle r^2 \rangle = (1 - f) N p_c l_c^{\,2} + f N l_h^{\,2} \frac{1 + \langle \cos\theta \rangle}{1 - \langle \cos\theta \rangle} \qquad (4)$$

where $\langle \cos\theta \rangle$ is the mean value of the cosine of the angle between end-to-end vectors of two helical monomer units. The value of $\langle \cos\theta \rangle$ assumes 1 or 0 for monomers in the same helical section or different helical sections, respectively. Therefore, $\langle \cos\theta \rangle = 1 \times (1 - p) + 0 \times p = 1 - p$, where $p$ is the probability of breaking the helix. $p$ is related to the average number of monomer units in a helical section as $\nu = 1/p$. Following Ptitsyn,[25] the following expression for the mean-square end-to-end distance can be derived:

$$\langle r^2 \rangle = N\left((1 - f) p_c l_c^{\,2} + 2 f l_h^{\,2} \nu \sqrt{\frac{f}{1 - f}}\right) \qquad (5)$$

The number of monomers in a Kuhn segment, $p_c$ and $\nu$ for helix and coil PLGA chains, respectively, were determined from atomistic MD simulations as detailed in Appendix B. A value of $p_c = 10$ is determined from MD simulations. The average number of monomers per helical section in the middle of the transition region is reported in the literature to be $\nu = 15$.[20] The MD simulations indicate that even in a fully protonated chain the average number of monomers in a helical segment is 15.

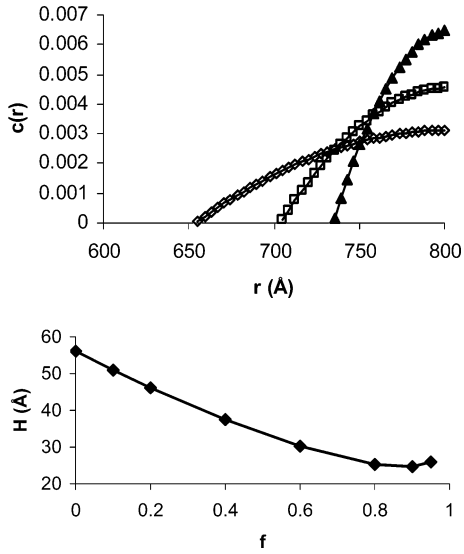


**Figure 1.** Results from mean-field calculations for grafted polypeptide chains. Top: monomer density (number/$l_c^3$) profile for $f = 0.95$ (filled triangles), 0.4 (open squares), and 0.0 (open diamonds). $r$ is the distance from the center of the pore. Bottom: variation of brush thickness $H$ with $f$. $R = 80$ nm, $N = 80$, and grafting density $= 0.05 l_c^{-2}$.

We now define the effective monomer repeat length and the Kuhn length as a function of $f$. A chain in the helix−coil transition region with both helical and random-coil units can be represented by a hypothetical chain that has an effective repeat length $a_{\text{eff}}$ and an effective Kuhn length of $p_{\text{eff}}$ residues and hence

$$\langle r^2 \rangle = N p_{\text{eff}} a_{\text{eff}}^{\,2} \qquad (6)$$

Approximating the value of $a_{\text{eff}}$ as the weighted average of helical and random coil repeat lengths, i.e., $a_{\text{eff}} = (1 - f) l_c + f l_h$, $p_{\text{eff}}$ can be determined by solving eq 5 and eq 6. The effective chain parameters were used as input in the mean-field calculation to determine $\Phi(r)$.

We have calculated the monomer density profile for a PLGA grafted inside a cylindrical nanopore of radius $R = 80$ nm as a function of $f$ by applying the method described in Appendix A. The values $N = 80$ and a grafting density $= 0.05 l_c^{-2}$ were used. The monomer density $c(r) = \Phi(r)/a_{\text{eff}}^3$ plotted in the top panel of Figure 1 for different values of $f$ shows spreading of the grafted layer as the helical content is decreased. This indicates that for the brush considered in the calculation increasing $f$ increases the pore opening. This is better illustrated by a plot of effective brush thickness defined as the first moment of $c(r)$

$$H = \frac{\int r c(r)\, \mathrm{d}r}{\int c(r)\, \mathrm{d}r} \qquad (7)$$

in the bottom panel of Figure 1.

It is important to point out that the Zimm−Bragg theory for the helix−coil transition is valid in the limit $N \gg 1$.[23] For low $N$ values the transition occurs in a wider pH range as compared to higher $N$ values. For $N$ values $< \nu$ (average number of monomers in a helical section in the middle of the transition region) a chain is either completely helical or completely coil; thus, in the middle of helix−coil transition region there are equal numbers of helical and coil chains. This changes fairly quickly with $N$. For example, Snipp et al.[28] have demonstrated that, in the case of PLGA, the helix−coil transition is very close to $N$

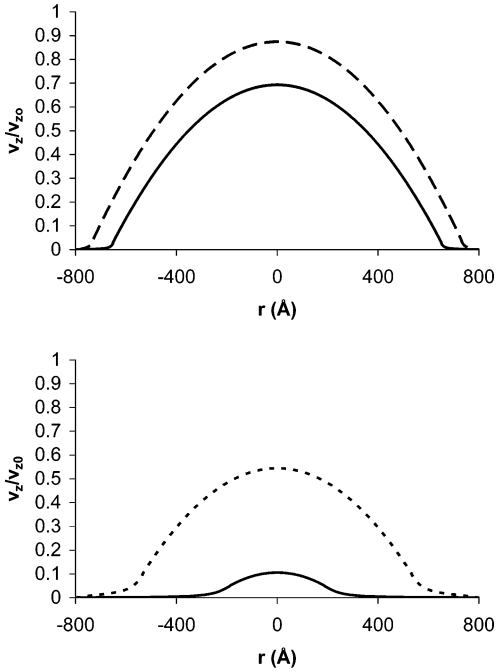


**Figure 2.** Normalized velocity profiles calculated using the Brinkman equation. $v_{z0}$ is the velocity at the center of the pore in an unmodified pore. The velocity profiles are for pH = 3 (broken line) and 7 (solid line) for a pore of $R = 800$ Å, grafting density $= 0.05l_c^{-2}$, $N = 80$ (top panel) and $N = 300$ (bottom panel).

≫1 behavior for chain lengths as low as 95. In this context, the use of Zimm−Bragg model for $N = 80$ in our calculations may be justified. However, it is desirable to study the effect of finite size on the monomer density profile and the applicability of the Zimm−Bragg model for grafted layers of much smaller chains.

**2.4. Calculation of the Velocity Profile.** Calculation of the velocity profiles used as an input $\Phi(r)$ obtained from the mean-field method explained in the preceding section. Because of the variation of polymer volume fraction as a function of $r$, eq 1 must be solved numerically. The calculation was performed by dividing the brush region into $n$ annular shells of thickness d$r$. A value of d$r = l_c$ was used. The Brinkman equation was written for $i = 1$, $n$ shells separately with permeability value $k_i$ related to the monomer density of the corresponding shell as $k_i = l_c^2/\Phi_i^2$.[15] For shells free of polymers, eq 1 reduces to the Navier−Stokes equation. The solution for the velocity profile involved making an initial guess for the velocity at the center of the pore. Equation 1 was then applied to shells $i = 1$ ($r = 0$) to $n$ ($r = R$) sequentially, subject to boundary conditions of constant velocity and shear stress at the interface between shell $i - 1$ and $i$ to obtain the velocity profile inside the pore. The composite velocity profile across the nanopore was obtained by successively improving the guess until the boundary condition that velocity at $r = R$ vanishes was met. As an example, the velocity profiles at pH values 3 and 7 for a pore of $R = 800$ Å, grafting density $= 0.05l_c^{-2}$, and degree of polymerization $N = 80$ (top panel) and $N = 300$ (bottom panel) are plotted in Figure 2. The velocity profile is normalized by $v_{z0}$, the velocity at the center of an unmodified pore under same flowing conditions.

## 3. Results

**3.1. Comparison with Experiments.** In their experiments, Park et al. measured a change in water permeability through a PLGA grafted nanoporous membrane as a function of pH.[1] The

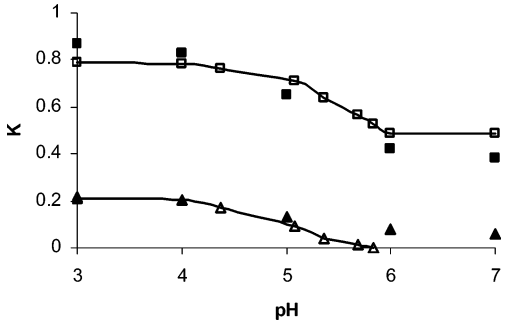


**Figure 3.** Comparison of results from continuum model and experiments. Plotted is the dimensionless permeability as a function of pH from continuum calculation and experiments.[1] Two systems investigated in ref 1 are considered: $N = 80$, grafting density $= 0.05l_c^{-2}$ (system A) and $N = 480$, grafting density $= 0.033l_c^{-2}$ (system B). System A: experimental (filled squares); theory (solid line with open squares). System B: experimental (filled triangles); theory (solid line with open triangles).

track etched porous polycarbonate membrane had an average pore diameter of 200 nm. The membrane was first coated with platinum and followed by gold. The thickness of the total coated metal was reported as 20 nm (therefore we use a pore radius $R = 80$ nm in our calculations). PLGA chains of length $N = 80$ or 480 residues, carrying a disulphide group at the $N$-terminal, were self-assembled on the metal-coated surface. The amount of PLGA ($N = 80$) and PLGA ($N = 480$) was $6 \times 10^{-11}$ and $4 \times 10^{-11}$ mol/cm$^2$, respectively. This corresponds to a distance between grafting points of 1.6 and 2.1 nm for $N = 80$ (system A) and $N = 480$ (system B), respectively. These corresponded to grafting densities $0.05l_c^{-2}$ and $0.033l_c^{-2}$ for systems A and B, respectively. We calculated the velocity profiles through nanoporous systems A and B at various values of $f$ using these grafting parameters and a value of $R = 80$ nm.

To compare the predictions of our model with the permeation experiments, the flow rate through the pore is extracted from the continuum velocity profile using the equation

$$Q = \int_0^R 2\pi r v_z(r)\, \mathrm{d}r \tag{8}$$

We define the dimensionless permeability of the pore $K = Q/Q_0$, where $Q_0$ is the flow rate through an unmodified pore of the same diameter under the same flow conditions. In Figure 3 we have compared $K$ as computed by the continuum analysis presented here and Park and co-workers' experiments. Results from our model agree very well with the experimental data. However, there is a slight discrepancy between theory and experiments that is more apparent at high pH values. This discrepancy between the results is reasonable considering the following simplifications made in our model. We have not included the effect of densely grafted chains on the helix−coil transition as well as on how helical segments are distributed along the chain. In particular, in the helix−coil transition regime, we have assumed that a monomer occurs in a helical conformation determined by $f$, independent of its position along the chain and the distance from the grafting point. Second, we have not considered the effect of counterion condensation. Despite these major simplifications, the model presented here is capable of accurately calculating flow control through the system.

**3.2. Designing a pH-Sensitive Flow Control Valve.** To design a smart flow control system, it is necessary to analyze the gating effect as a function of pore size, degree of polymerization, and grafting density. The performance of the

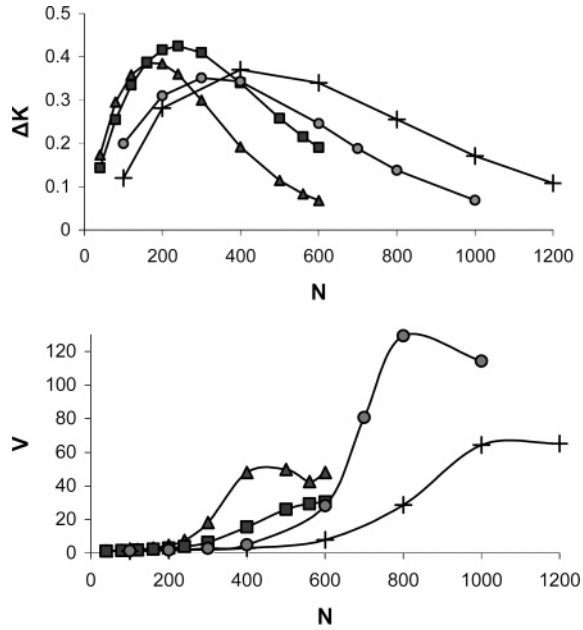


**Figure 4.** Smart nanovalve performance characteristics. $\Delta K = K_{pH=3} - K_{pH=7}$ (top) and $V = K_{pH=3}/K_{pH=7}$ (bottom) as a function of $N$ for grafting densities $0.05l_c^{-2}$ (triangles) and $0.025l_c^{-2}$ (squares) at $R =$ 800 Å and $0.05l_c^{-2}$ (circles) and $0.025l_c^{-2}$ (crosses) at $R = 1600$ Å.

nanoporous system at a given grafting condition is determined by the maximum change in permeability between the closed and open states. We characterize the change in solvent permeability by two quantities: the difference $\Delta K$ and the ratio $V$ between permeability values at pH = 3 and 7. The second quantity $V$ is termed as the *valve effect*. In the top panel of Figure 4, $\Delta K = K_{pH=3} - K_{pH=7}$ is plotted as a function of the degree of polymerization $N$ for two different grafting densities in pores of $R = 800$ and 1600 Å. At low degrees of polymerization the value of $\Delta K$ increases with $N$. When the grafted layer thickness in the closed state is comparable to the pore radius, an increase in $N$ continues to decrease $K$ in the open state without causing comparable reduction in $K$ in the closed state. Consequently, $\Delta K$ reaches a maximum value and then begins to decrease with increasing $N$ as indicated by the results. The $N$ value at which $\Delta K$ reaches a maximum increases with decreasing grafting density and increasing $R$. The valve effect $V$ as a function of $N$ is plotted in the bottom panel of Figure 4 for the above parameters. The valve effect $V$ increases with $N$, reaches a maximum, and then starts to decrease. The maximum in $V$ reaches at a higher $N$ value as compared to the maximum in $\Delta K$. It is noted that the maximum change in permeability is obtained when the outer edge of the grafted layer (marked by $\Phi(r) = 0$) in the closed state coincides with the pore center. In designing a smart nanoporous system, the choice of grafting parameters should depend on the specific application.

A simple analysis to characterize the variation of valve effect as a function of $N$ can be put forward as follows. From the well-known equations of fluid mechanics, the valve effect is given by

$$V = \left(\frac{R - H_{pH=3}}{R - H_{pH=7}}\right)^4 \tag{9}$$

The change in grafted layer thickness due to a coil−helix transition is given by $\Delta H = H_{pH=7} - H_{pH=3}$.Using polymer brush scaling laws[29] and neglecting the effect of concavity of the grafting surface, the change in average thickness of the grafted layer can be approximated as

$$\Delta H \approx N\rho^{1/3}(a_{pH=7} - a_{pH=3}) \tag{10}$$

where $\rho$ is the grafting density. Thus, the valve effect can be approximated as

$$V \approx \theta = \left(\frac{R - xH_{pH=7}}{R - H_{pH=7}}\right)^4 \tag{11}$$

where $x = a_{pH=3}/a_{pH=7}$ is the ratio of effective monomer length as given in section 2.3. In Figure 5 the valve effect is replotted against $\theta$ using a value of $x = 0.42$. The plots for two different grafting densities at two $R$ values collapse onto a single master curve for values of $\theta$ below 2. This indicates that the simple description in eq 11 captures the gating effect fairly well for low $\theta$ values. For $\theta$ values above that corresponding to $R/H_{pH=7} \sim 1$, the grafted layer thickness does not increase any further and hence the deviation from the master curve.

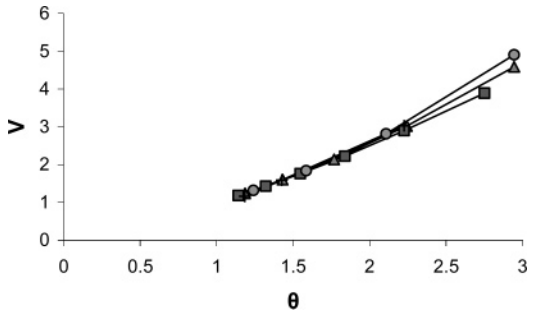


**Figure 5.** $V$ as a function of $\theta$ for grafting densities $0.05l_c^{-2}$ (solid triangles) and $0.025l_c^{-2}$ (solid squares) at $R = 800$ Å and $0.05l_c^{-2}$ (solid diamonds) and $0.025l_c^{-2}$ (+) at $R = 1600$ Å.

## 4. Conclusions

In this article, a powerful combination of polymer statistical physics, molecular simulation, and continuum fluid mechanics is applied to analyze water permeation control through a nanoporous membrane grafted with poly(L-glutamic acid) chains. We have analyzed the helix−coil transition according to the Zimm−Bragg model to determine the monomer density profile of the grafted polypeptide layer inside a cylindrical nanopore as a function of pH. We have then calculated the flow rate through the nanopore as a function of pH. The results are compared with recent experiments by Park and co-workers.[1] These calculated permeability change was in very good agreement with experimental values. The findings establish that polymer statistical mechanical models combined with a continuum porous layer treatment of flow through the polypeptide grafted nanopore can be used successfully to model smart flow control systems. The effect of grafting parameters on permeability change was analyzed. The optimum grafting parameters correspond to those for which the span of the monomer density profile is approximately equal to the pore radius in the closed state. The method described here can be easily extended to other polymer−solvent systems.

## Appendix A. Calculation of $\Phi(r)$ by Mean-Field Brush Models

To calculate $\Phi(r)$, we have extended the mean-field analytic theory of Zhulina and co-workers[17] developed for planar brushes to the case of a concave cylindrical brush. We consider PLGA chains of length $N$ monomers grafted to an impermeable concave

cylindrical surface of radius $R$, with a grafting density of one chain per an area of $s$. The monomer size and the number of residues in the Kuhn segment are taken as the effective monomer size $a_{eff}$ and the number of residues $p_{eff}$ in effective Kuhn length, respectively, as described in section 2.3. The quantity $r$ is the radial distance measured from the axis of the cylinder, and $h = R - r$ is the distance from the grafting surface.

The equilibrium monomer density profile, or alternatively monomer volume fraction as a function of distance from grafting surface, $\phi(h)$, in the brush layer can be determined by minimizing its total conformational free energy

$$\Delta F = \Delta F_{conc} + \Delta F_{el} \tag{A.1}$$

which contains the volume interaction energy

$$\Delta F_{conc} = \frac{s}{a_{eff}^3 R}\int_0^H \upsilon\phi^2(h)(R-h)\,dh \tag{A.2}$$

and elastic stretching energy

$$\Delta F_{el} = \frac{3}{2p_{eff}a_{eff}^2}\int_0^H g(h')\,dh'\int_0^{h'} E(h,h')\,dh \tag{A.3}$$

where the function $g(h')$ is the average fraction of chains ending at a radial distance $h'$ and $E(h,h')$ gives the local stretching $dh/dn$ at $h$ for a chain ending at $h'$. The parameter $\upsilon = \pi a_{eff}^3/6$ represents the excluded volume. The volume fraction of monomers $\phi(h)$ is expressed by the functions $g(h')$ and $E(h,h')$ as

$$\phi(h) = \frac{a_{eff}^3 R}{s(R-h)}\int_h^H \frac{g(h')}{E(h,h')}\,dh' \tag{A.4}$$

Minimizing the free energy $\Delta F$ as a functional of unknown functions $g(h')$ and $E(h,h')$ under the constraints

$$\frac{s}{a_{eff}^3 R}\int_0^H \phi(h)(R-h)\,dh = N \tag{A.5}$$

and

$$\int_0^{h'} \frac{1}{E(h,h')}\,dh = N \tag{A.6}$$

gives the expression for the function of local chain stretching

$$E(h,h') = \frac{\pi}{2N}\sqrt{h'^2 - h^2} \tag{A.7}$$

and for volume fraction of monomers in a layer

$$\phi(h) = \frac{1}{2\upsilon}(-K^2h^2 - \lambda) \tag{A.8}$$

where

$$K^2 = \frac{3\pi^2}{8N^2 a_{eff}^2} \tag{A.9}$$

and $\lambda$ is a undetermined Lagrangian multiplier that can be determined from the normalization of eq A.5. The function $g(h')$ can then be determined by solving the integral equation (A.4), with $g(h')$ as an unknown function. Equations A.7, A.2, and A.3 were then used to determine the free energy $\Delta F$ as a function of height $H$. The equilibrium value of brush height, $H_0$, was determined by minimizing the free energy with respect to $H$. Once $H_0$ is known, the monomer volume fraction profile is easily computed.

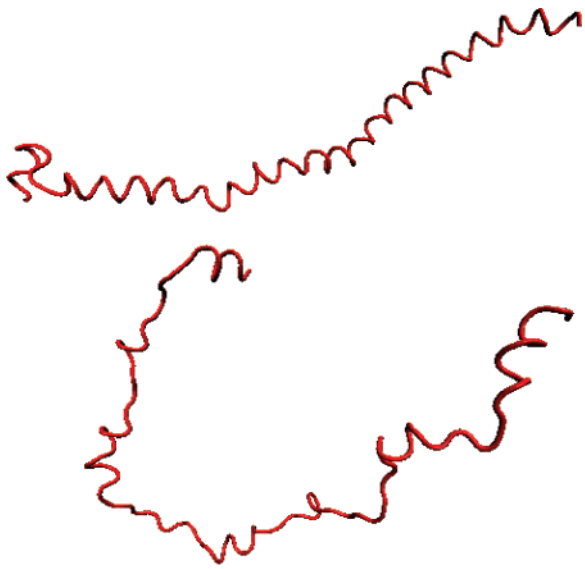

**Figure 6.** Ribbon models of protonated (top) and deprotonated (bottom) poly(L-glutamic acid) chains generated from MD simulations. $N = 80$.

## Appendix B. Molecular Dynamics Simulations of Protonated and Deprotonated PLGA Chains

Molecular dynamics (MD) simulations were carried out to extract chain parameters of isolated PLGA molecules in water. Two systems corresponding to PLGA in the protonated ($PLGA_p$) and deprotonated ($PLGA_{dp}$) states were studied using MD simulations. Each system consisted of an 80-residue-long PLGA chain, of which the N-terminus and C-terminus were acytylated and methyl-amidated, respectively. The all-atom parametrization of the AMBER force field was used in the simulations. The initial model of the chain was built using the LEAP module of Amber7.[30] The residues GLH and GLU corresponding to the protonated and deprotonated states, respectively, are included in the Amber library. The $PLGA_p$ chain consisted of all protonated residues, and the $PLGA_{dp}$ chain consisted of all deprotonated residues. The completely stretched initial model of the chain was energy-minimized for 2000 steps to remove any unfavorable contacts between atoms. The minimized structure was then immersed into a box of water molecules having a density of 1 g/cm$^3$. TIP3P water was used as the water model. Monovalent counterions ($Na^+$) were included such that the net charge of the system was zero. The numbers of counterions included were 2 and 80 for $PLGA_p$ and $PLGA_{dp}$ systems, respectively. A time step of 1.0 fs was used in the simulations. The systems were equilibrated at a temperature of 300 K for about 50 ps. This was followed by a MD simulation of 1.5 ns. Sampling was begun after 500 ps.The $PLGA_p$ chain formed a predominantly helical (>85% residues in the helical state) structure. It is reported in the literature that PLGA does not reach 100% helical content even at saturation pH at room temperature.[28] The helical segments in the simulated chain contained 15 residues on an average. As was expected, the $PLGA_{dp}$ chain formed a random coil. The number of residues in Kuhn segment for the coil was calculated to be ~10 residues, using the wormlike chain model.[31] The $PLGA_p$ (top panel) and $PLGA_{dp}$ (bottom panel) chains are represented by ribbon models in Figure 6.

**Acknowledgment.** This work was supported in part by NASA-Ames through a NASA−North Carolina State University cooperative research agreement and by the National Science Foundation through Grant CTS-0403633.

## References and Notes

(1) Park, Y. S.; Toshihiro, I.; Imanishi, Y. *Langmuir* **2000**, *16*, 5376.
(2) Akerman, S.; Viinikka, P.; Svarfvar, B.; Putkonen, K.; Jarvinen, K.; Kontturi, K.; Nasman, J.; Urtti, A.; Paronen, P. *Int. J. Pharm.* **1998**, *164*, 29.
(3) Lokuge, I.; Wang, X.; Bohn, P. W. *Langmuir* **2007**, *23*, 305.
(4) Yu, C.; Mutlu, S.; Selvaganapathy, P.; Mastrangelo, C. H.; Svec, F.; Fréchet, J. M. J. *Anal. Chem.* **2003**, *75*, 1958.
(5) Mika, M.; Childs, R. F.; Dickson, J. M. *J. Membr. Sci.* **1999**, *153*, 45.
(6) Beebe, D. J.; Moore, J. S.; Bauer, J. M.; Yu, Q.; Liu, R. H.; Devadoss, C.; Jo, B. H. *Nature (London)* **2000**, *404*, 588.
(7) Park, Y. S.; Ito, Y.; Imanishi, Y. *Macromolecules* **1998**, *31*, 2606.
(8) Hollman, A. M.; Bhattacharyya, D. *Langmuir* **2002**, *18*, 5946.
(9) Davis, M. E. *Microporous Mesoporous Mater.* **1998**, *21*, 173.
(10) Adiga, S. P.; Brenner, D. W. *Nano Lett.* **2005**, *5*, 2509.
(11) Huang, J.; Wang, Y.; Laradji, M. *Macromolecules* **2006**, *39*, 5546.
(12) Tessier, F.; Slater, G. W. *Macromolecules* **2006**, *39*, 1250.
(13) Zimm, B. H.; Bragg, J. K. *J. Chem. Phys.* **1959**, *31*, 526.
(14) Brinkman, H. C. *Appl. Sci. Res.* **1947**, *A1*, 27.
(15) Milner, S. T. *Macromolecules* **1991**, *24*, 3704.
(16) Milner, S. T. *Science* **1991**, *251*, 905.
(17) Zhulina, Y. B.; Pryamitsyn, V. A.; Borisov, O. V. *Polym. Sci. U.S.S.R.* **1989**, *31*, 205.
(18) Field, J. B.; Toprakcioglu, C.; Ball, R. C.; Stanley, H. B.; Dai, L.; Barford, W.; Penfold, J.; Smith, G.; Hamilton, W. *Macromolecules* **1992**, *25*, 434.
(19) Karim, A.; Sajita, S. K.; Douglas, J. F.; Ankner, J. F.; Fetters, L. J. *Phys. Rev. Lett.* **1994**, *73*, 3407.
(20) Poland, D.; Scheraga, H. A. *Theory of Helix-Coil Transitions in Biopolymers*; Academic Press: New York, 1970.
(21) Zhang, W.; Nilsson, S. *Macromolecules* **1993**, *26*, 2866.
(22) Pauling, L.; Corey, R. B.; Branson, H. R. *Proc. Natl. Acad. Sci. U.S.A.* **1951**, *37*, 205.
(23) Birshtein, T. M.; Ptitsyn, O. B. *Conformations of Macromolecules*; Interscience Publishers: New York, 1966; Chapter 9.
(24) Grosberg, Y.; Khokhlov, A. R. *Statistical Physics of Macromolecules*; AIP Press: New York, 1994; Chapter 7.
(25) Ptitsyn, O. B. In Ramachandran, G. N., Ed. *Conformation of Biopolymers*; Academic Press: New York, 1967; Vol. 1, p 381.
(26) Wang, Y.; Chang, Y. C. *Macromolecules* **2003**, *36*, 6503.
(27) Buhot, A.; Halperin, A. *Europhys. Lett.* **2000**, *50*, 756.
(28) Snipp, R. L.; Miller, W. G.; Nylund, R. E. *J. Am. Chem. Soc.* **1965**, *87*, 3547.
(29) de Gennes, P. G. *Macromolecules* **1980**, *13*, 1069.
(30) Case, D. A.; et al. AMBER 7, University of California, San Francisco, 2002. Pearlman, D. A.; et al. AMBER, a package of computer programs for applying molecular mechanics, normal mode analysis, molecular dynamics and free energy calculations to simulate the structural and energetic properties of molecules. *Comput. Phys. Commun.* **1995**, *91*, 1.
(31) Flory, P. F. *Statistical Mechanics of Chain Molecules*; Interscience Publications: New York, 1969; Chapter 7.

MA0617522